Journal of Sound and Vibration 362 (2016) 39–55

Contents lists available at ScienceDirect

Journal of Sound and Vibration

journal homepage: www.elsevier.com/locate/jsvi

Noise control of dipole source by using micro-perforated panel housing

Q. Xi [a], Y.S. Choy [a,*], L. Cheng [a], S.K. Tang [b]

[a] Department of Mechanical Engineering, The Hong Kong Polytechnic University, Hung Hom, Kowloon, Hong Kong
[b] Department of Building Services Engineering, The Hong Kong Polytechnic University, Hung Hom, Kowloon, Hong Kong

ARTICLE INFO

Article history:
Received 22 December 2014
Received in revised form
19 September 2015
Accepted 28 September 2015
Handling Editor: Y. Auregan
Available online 31 October 2015

ABSTRACT

Mitigating low-frequency noise in a small ducted fan system such as hairdryer is still a technical challenge. Traditional duct lining with porous materials work ineffectively due to the limitation of its thickness and length of small domestic product with ducted fans. This study presents a passive approach to directly suppress the sound radiation from the fan housed by a short microperforated panel covered with a shallow cavity backing. The noise suppression is achieved by the sound cancellation between sound fields from a fan of a dipole nature and sound radiation from a vibrating panel via vibro-acoustic coupling and by sound absorption in micro-perforations to widen the stopband. A two-dimensional theoretical model, capable of dealing with strong coupling among the vibrating micro-perforated panel, sound radiation from the dipole source, sound fields inside the cavity and the duct is developed. Through modal analysis, it is found that the even modes of the panel vibration are very important to cancel the sound radiation from the dipole source. Experimental validation is conducted with a loudspeaker to simulate the dipole source, and good agreement between the predicted and measured insertion loss (IL) is achieved.

1. Introduction

Fan installed in duct with a low aspect ratio can often be found in domestic and industrial applications, for example, the driving fan in ventilation system or the cooling fan in computers or turbo-fans in aircrafts. When the fan operates at low rotational speed such as in domestic product, the low frequency noise component is normally dominant and it is very annoying. The ducted fan noise can be mitigated in the propagating path or directly on the noise source itself. For the first approach such as in the ductwork of central air conditioning systems, porous materials lining the duct wall [1,2] have been frequently adopted to absorb the noise, but it only works well at high frequencies and the fibrous materials may cause environmental problems such as accumulation of dust due to its low durability. Besides, the concept of expansion chamber [3,4] or multiple chambers with perforated tubes [5] are commonly implemented in exhaust system in vehicles. It can abate the noise at a desirable frequency range but it will be very bulky for controlling the low frequency region. In addition, there is also significant pressure loss in a flow duct due to the sudden expansion and blockage of flow attributed to the internal tubes.

* Corresponding author.
E-mail address: mmyschoy@polyu.edu.hk (Y.S. Choy).

http://dx.doi.org/10.1016/j.jsv.2015.09.047
0022-460X/

Aiming to design a broadband passive noise control device that works effectively in the low-to-medium frequency range with negligible pressure drop, Huang introduced the concept of a drum-like silencer [6] which is formed by an expansion chamber with light membranes covering the side-branch cavities under fairly high tension. To ease the installing process without any machine for exerting force, the membrane has been replaced by a plate [7] and non-uniform plate [8]. In order to further improve the silencing performance, the plate with perforations [9] which is the so-called micro-perforated panel (MPP) has been adopted. The MPP was proposed by Maa [10–12] and is widely used in different areas such as room acoustics [13], barrier design [14] and duct mufflers [9,15–18]. A typical MPP absorber takes the form of a MPP in front of backing cavity that can only provide efficient sound absorption within a rather narrow frequency band. The vibro-acoustic behavior of thin and flexible MPPs has been studied by Bravo [19,20]. To broaden the effective frequency band, it is possible to reduce the size of perforations [12] or adopt MPP with an irregular cavity [21] which was investigated theoretically and validated by experiment with normal incidence of sound wave. Subsequently, a wider absorption bandwidth was achieved due to the increased vibro-acoustic coupling between the cavity and air motion in the MPP. In order to obtain broader absorption band, recently some researchers introduce a device which consists of a micro-perforated panel (MPP) backing with cavity array [15,22]. Compared with single MPP absorber, the device can provide significantly better sound absorption performance over a broad frequency band. This is not only attributed to the combination of different resonances of MPP with each cavity, but also the frequency shifts due to inter-resonator interactions [22].

Such parallel-arranged MPP absorber array was recently examined at oblique incidence and in diffuse field. The sound absorption of this MPP absorber array with periodic arrangement can be maintained in a wide frequency range in diffuse field [23]. For the theoretical study of the sound absorption of a finite flexible MPP backed by an air cavity, the team of Lee developed a solution procedure based on the modal analysis approach [24]. The theoretical model established takes into account the full coupling between the sound wave in the cavity and the panel vibration. It assumes a rectangular cavity and the exterior acoustic loading on the MPP surface is simplified as a uniformly distributed sound pressure. However, when vibro-acoustic coupling between the light MPP and cavity with irregular shape is investigated, the exterior acoustic loading is non-uniform due to the radiation pressure from the MPP. In addition, the acoustic mode of the cavity in irregular shape is needed to be found by numerical method instead of directly adopting this modal analysis approach [21]. Besides, many researchers considered the uniform incident pressure when they studied the performance of MPP absorbers [21,24,25] and then their theoretical models are limited to predicting the performance of MPP backed with a cavity that is far away from the sound source.

Practically, due to the limitation of space or duct length, the silencer is frequently installed close to the sound source, such as a fan. As a result, the incident pressure excitation on the silencer surface is non-uniform. In addition, the sound wave from a real-life fan blade can be modeled as a dipole source [3]. In this regard, the team of Liu recently introduced a passive method to suppress the subsonic axial fan noise of dipole nature by membrane housing through the interaction between membrane vibration and the sound fields in the duct and cavities via vibro-acoustic coupling, undergoing sound cancellation [26]. The proposed noise control device with tensioned membrane can achieve 10 dB of IL with a stopband wider than an octave, but the geometry is not compact and there is a need for installing a special machine on the duct to apply tensile force on the membrane. To solve both problems, the membrane is replaced by a micro-perforated plate which can undergo sound cancellation with the sound radiation from the fan of dipole nature and supplemented with sound absorption to widen the stopband in a more compact geometry. Therefore the objectives of the current study are (1) To establish a theoretical model which allows a thorough analysis on the vibro-acoustic coupling among the MPP vibration, the non-uniform incident pressure excitation from a dipole sound source, the sound fields in the duct, and the acoustic waves inside the cavity. (2) To understand the physics behind the achievement of a wide stopband by the combination of sound cancellation and sound absorption due to the coupling between the MPP and dipole source. It is expected that the MPP housing device will outperform the device of tensioned membrane with side-branch cavities which only involves sound cancellation mechanism. (3) To further investigate the performance of the MPP housing device on sound sources of different nature (i.e., monopole and dipole). This is because the real-life fan is not a pure dipole, and the design of the MPP housing device will be different for controlling the combination of monopole and dipole source.

In what follows, Section 2 outlines the analytical model for a cavity-backed MPP with dipole sound waves excitation at the center of the MPP housing device. Section 3 focuses on the numerical validation, optimization process, and understandings of the mechanism of noise suppression by using MPP housing. The experimental validation of the theoretical model is described in Section 4 and the main conclusions is given in Section 6.

2. Theoretical modeling

A two-dimensional model of a cavity-backed MPP housing a dipole sound source is shown in Fig. 1. It consists of a rectangular duct of height h^*, and two rigid side-branch cavities of length L_c^* and depth h_c^*. The cavities are covered by two pieces of MPP which are equal to the cavity length with fixed boundary support. A dipole source which is applied to simulate fan noise is located at the mid-point of the MPP; $x^*=0.5L^*$, $y^*=0.5h^*$. For convenience, all variables are non-

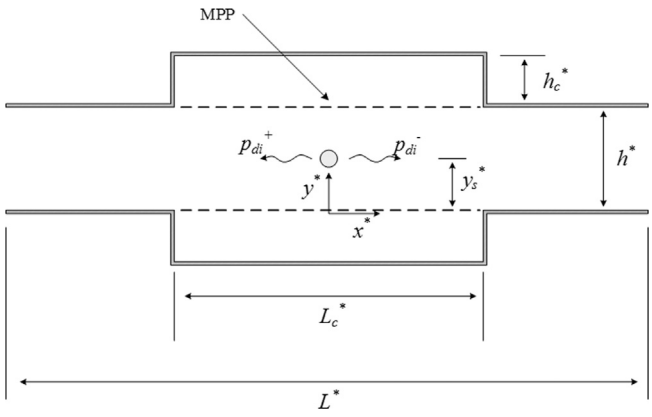

Fig. 1. 2D theoretical model of the dipole noise control by the MPP housing.

dimensionalized by three basic quantities, air density ρ_0^* , duct height h^* and speed of sound in free space c_0^* as follows:

$$x=\frac{x^*}{h*},\quad y=\frac{y^*}{h*},\quad h_c=\frac{h_c{}^*}{h*},\quad L=\frac{L^*}{h*},\quad L_c=\frac{L_c{}^*}{h*}$$

$$f=\frac{f^*h^*}{c_0^*}\ ,\quad \omega=\frac{\omega^*h^*}{c_0^*}\ ,\quad k_0=2\pi f\ ,\quad m=\frac{m^*}{\rho_0^*h^*}$$

$$B=\frac{B^*}{\rho_0^*c_0^{*2}h^{*3}},\quad F=\frac{F^*}{h^*\rho_0^*(c_0^*)^2}\ ,\quad p=\frac{p^*}{\rho_0^*(c_0^*)^2}$$

where m is the plate-to-air mass ratio, B is the dimensionless bending stiffness of the plate, F is the concentrated force exerted on the fluid by the dipole source and p is the sound pressure. Based on such a normalization scheme, the first cut-on frequency of the rigid-walled duct is $f=0.5$.

The dipole sound waves p_d radiated from the mid-point to upstream for $x<0.5L$ and downstream side for $x>0.5L$ inside a duct is expressed as [27]

$$p_d=\sum_{n=0}^{\infty}\frac{(2-\delta_{0n})F\ \cos(n\pi/2)\cos(n\pi y)}{(1-M^2)(k_n^+-k_n^-)}\left[k_n^+e^{ik_n^+(x-0.5L)}H(x-0.5L)+k_n^-e^{ik_n^-(x-0.5L)}H(0.5L-x)\right]$$

$$k_n^{\pm}=\mp\frac{-k_0M-i\sqrt{(1-M^2)(n\pi/h)^2-k_0^2}}{1-M^2} \tag{1}$$

where $H(x)$ is the Heaviside function, δ_{0n} is Kronecker delta function, M is the Mach number, $k_0=\omega/c_0$ is the wave-number, ω is the angular frequency, c_0 is the speed of sound and n is any integer.

The radiated sound waves from the dipole source excite the panel into vibration with a transverse displacement of complex amplitude η in the y direction with velocity $v_p=\partial\eta/\partial t$. The vibrating panel radiates sound into the duct and cavity which are denoted by p_{rad} and p_{cav} respectively. The vibration of the panel at $y=0$ with the pressure difference between the duct and the cavity is governed by

$$\frac{B}{i\omega}\frac{\partial^4v_p}{\partial x^4}+mi\omega v_p+p_d+p_{rad}-p_{cav}=0\quad . \tag{2}$$

Considering the micro-perforation in the MPP, as a lattice of sub-millimeter holes uniformly distributed over the surface of the plate, the sound pressure difference applied between the two sides of the plate generates air mass vibration in the holes. As the orifice diameter is much smaller than the wavelength of the impinging acoustic waves, the air particle velocity is assumed to be distributed uniformly within the area of each hole. The air and structure interaction is given by [28]

$$Z_{i,resist}(v_0-v_p)+Z_{i,react}v_0+(p_d+p_{duct}-p_{cav})=0 \tag{3}$$

with the impedance of MPP for grazing flow effect [29]

$$Z_{i,resist}=\frac{32\mu t}{\sigma\rho_0c_0d^2}\left[\left(1+\frac{K^2}{32}\right)^{1/2}+\frac{\sqrt{2}}{32}K\frac{d}{t}\right]+\frac{2\alpha R_s}{\sigma\rho_0c_0}+\frac{|u_h|}{\sigma c_0}+\frac{0.15M}{\sigma}\ \text{and} \tag{4}$$

$$Z_{i,react} = i \cdot \frac{\omega t}{\sigma c_0}\left[1+\left(1+\frac{K^2}{32}\right)^{-1/2}+0.85\frac{d}{t}\right] + \frac{0.85 d\omega F_\delta}{\sigma c_0\left(1+\frac{|u_h|}{\sigma c_0}\right)}. \tag{5}$$

where v_0 is the particle velocity of fluid in the holes, $K = d\sqrt{\omega\rho_0/4\mu}$, $R_s = 0.5\sqrt{2\mu\omega\rho_0}$, d is the hole diameter, t is the panel thickness, σ is the perforated ratio, μ is the coefficient of viscosity, α is a factor which is equal to 2 for rounded edge holes, u_h is the absolute value or the peak particle velocity inside the holes and $F_\delta = (1+(12.6M)^3)^{-1}$. The real part $Z_{i,resist}$ is called the acoustic resistance which is associated with the energy radiation and viscous losses. The imaginary part $Z_{i,react}$ is called the acoustic reactance which is inertial in nature. For the case without flow, only the first two terms of $Z_{i,resist}$ in Eq. (4) and first term of $Z_{i,react}$ in Eq. (5) are considered as the impedance of MPP.

The average velocity distribution for the whole plate with micro-perforations, $\overline{V}(x)$, is defined as $\overline{V}(x) = (1-\sigma)v_p(x)+\sigma v_0(x)$. Eqs. (2) and (3) can be solved by the standard Galerkin procedure and v_p is expanded as a series of in-vacuo modes φ_j by clamped–clamped MPP with modal amplitude $V_{p,j}$,

$$v_p(x) = \sum_{j=1}^{\infty} V_{p,j}\varphi_j(\xi), \xi = x/L+1/2;$$

$$\text{where } \phi_j(\xi) = \frac{1}{2}(1-\varepsilon_j)e^{\lambda_j\xi}+\frac{1}{2}(1+\varepsilon_j)e^{-\lambda_j\xi}+\varepsilon_j \sin(\lambda_j\xi) - \cos(\lambda_j\xi);$$

$$\text{with } \varepsilon_j = \frac{\cosh(\lambda_j)-\cos(\lambda_j)}{\sinh(\lambda_j)-\sin(\lambda_j)}, \cos(\lambda_j)\cosh(\lambda_j) = 1. \tag{6}$$

Similarly, the mean velocity of surrounding air $\overline{v}_0 = \sigma v_0$, can also be expanded over the same series $\phi_j(\xi)$ as

$$\overline{v}_0(x) = \sum_{j=1}^{\infty}\overline{V}_{0j}\varphi_j(\xi), \quad v_0 = \sum_{j=1}^{\infty} V_{0j}\varphi_j(\xi), \quad \text{with } V_{0,j} = \frac{\overline{V}_{0j}}{\sigma}. \tag{7}$$

Hence, Eqs. (2) and (3)become

$$\left\{\frac{B}{i\omega}\left(\frac{\lambda_j}{L}\right)^4 + mi\omega\right\}V_{p,j} + \int_0^1 (p_d+p_{rad}-p_{cav})\varphi_j(\xi)d\xi = 0, \tag{8}$$

$$Z_{i,resist}(V_{0,j}-V_{p,j}) + Z_{i,react}V_{0,j} + \int_0^1 (p_d+p_{rad}-p_{cav})\varphi_j(\xi)d\xi = 0. \tag{9}$$

respectively

The radiated pressure in the duct P_{rad} from the plate at $y=0$ can be calculated as [30]

$$p_{rad}(x,y) = \frac{L}{2}\sum_{n=0}^{\infty} c_n\psi_n(y) \times \int_0^1 \overline{V}(x')\psi_n(0)[H(x-x')e^{-ik_n(x-x')}+H(x'-x)e^{+ik_n(x-x')}]d\xi' \tag{10}$$

$$\text{with } c_n = \frac{i}{\sqrt{(n\pi/\omega)^2-1}}, k_n = \frac{\omega}{c_n}, \psi_n = \sqrt{2-\delta_{0n}}\cos(n\pi y) \tag{11}$$

and c_n, k_n, ψ_n are the modal phase speed, the modal wavenumber, and the modal velocity potential respectively. The value of x' varies within the range of $[-L/2, L/2]$.

The sound pressure inside the cavity can be expressed in terms of acoustic modes r and s of rigid-walled cavity with light damping [31]:

$$P_{cav}(x,y) = \sum_{r,s}^{\infty}\frac{-i\omega\phi_{rs}(x,y)}{L_c h_c(\kappa_{r,s}^2-k^2+2i\zeta_{r,s}\kappa_{r,s}k)}\int_0^1 \overline{V}(x',0)\phi_{rs}(x',0)\mathrm{d}x'$$
$$V(x',0) \tag{12}$$

$$\text{with } \phi_{rs}(x,y) = \sqrt{(2-\delta_{0r})(2-\delta_{0s})}\cos\left(\frac{r\pi x}{L_c}\right)\cos\left(\frac{s\pi y}{h_c}\right), \kappa_{rs} = \sqrt{\left(\frac{r\pi}{L_c}\right)^2+\left(\frac{s\pi}{h_c}\right)^2} \tag{13}$$

where $\zeta_{r,s}$ is the damping ratio of the (r,s) acoustics mode, and $\kappa_{r,s}$ is the corresponding acoustic wavenumber.

The modal coefficient of dipole sound waves $I_{d,j}$, the duct modal impedance $Z_{rad,j}$ and the cavity modal impedance $Z_{cav,j}$ are defined as

$$I_{d,j} = \int_0^1 p_d\varphi_j(\xi)d\xi, \; Z_{rad_j} = \int_0^1 p_{rad}\varphi_j(\xi)d\xi, Z_{cav_j} = \int_0^1 p_{cav}\varphi_j(\xi)\mathrm{d}\xi. \tag{14}$$

As a result, Eqs. (8) and (9) become

$$[(B/i\omega)(\lambda_j/L)^4+mi\omega]V_{p,j}+(Z_{rad}-Z_{cav})[(1-\sigma)V_{p,j}+\sigma V_{0,j}] = -I_{d,j}, \tag{15}$$

$$Z_{i,resist}(V_{0,j}-V_{p,j})+Z_{i,react}V_{0,j}+(Z_{rad}-Z_{cav})((1-\sigma)V_{p,j}+\sigma V_{0,j})=-I_{d,j} \tag{16}$$

respectively.

Eqs. (15) and (16) are expressed in matrix format,

$$\begin{bmatrix} (B/i\omega)(\lambda_j/L)^4+mi\omega+(Z_{rad}-Z_{cav})(1-\sigma) & \sigma(Z_{rad}-Z_{cav}) \\ -Z_{i,resist}+(Z_{rad}-Z_{cav})(1-\sigma) & Z_{i,resist}+Z_{i,react}+\sigma(Z_{rad}-Z_{cav}) \end{bmatrix} \begin{bmatrix} V_{p,j} \\ V_{0,j} \end{bmatrix} = -\begin{bmatrix} I_{d,j} \\ I_{d,j} \end{bmatrix} \tag{17}$$

Having performed the transformation, the mode amplitudes $V_{p,j}$ and $V_{0,j}$ can be obtained. Then the sound pressure transmitted to the upstream and downstream of the duct can be expressed as

$$P_{radup}(x,y)|_{n=0,x\to-\infty}=\frac{L}{2}\sum_{j=1}^{\infty}V_j\int_0^1\varphi_j(\xi)e^{ik_0(x-x')}d\xi' \tag{18}$$

$$\text{and } P_{raddn}(x,y)|_{n=0,x\to+\infty}=\frac{L}{2}\sum_{j=1}^{\infty}V_j\int_0^1\varphi_j(\xi)e^{-ik_0(x-x')}d\xi' \text{ respectively.} \tag{19}$$

Eqs. (1)–(19) are solved in a coupled manner and the sound insertion loss (IL) defined as the acoustical power loss resulting from insertion of silencing device is computed by integrating the sound energy at the exits of straight duct with uniform cross-sectional area to obtain a reference value and then subtracting the integration result of sound energy at silenced duct outlets with exactly the same cross-sectional area and duct length.

$$\mathrm{IL}=10\log 10\left(\frac{\int_{str}|p|^2\mathrm{d}s}{\int_{mpp}|p|^2\mathrm{d}s}\right) \tag{20}$$

where s is the cross section area, p is the pressure at the duct outlets, the "*str*" refers to the straight duct without the MPP housing device, and "*mpp*" refers to the duct with MPP and backing cavities.

3. Numerical results and discussion

The analytical model is mainly used to help understanding the vibro-acoustic coupling among the acoustic field in duct, cavity and the panel vibration in a mathematical way. For the purpose of visualization of pressure and intensity field inside the housing, there is a need to adopt the finite element tool for numerical simulation. The commercial software Comsol Multiphysics® for numerical simulation is employed because of its strong multi-physics capability. In the numerical simulation, there are two domains. One is a two-dimensional domain for fluid to describe the sound wave propagation in the duct and cavity. Another is the one-dimensional domain for the structural vibration of the beam with micro-perforation properties. With the duct length $L=6.2$ and height $h=1$, cavity length $L_c=3$ and height $h_c=0.5$, the device has the expansion ratio of 2. There are 5400 triangular elements for the duct as well as the cavities with mesh size 0.1 which is the dimensionless length of each triangular mesh element. For the microperforated beam, mesh size 0.01 and 300 nodes are used. In the analytical calculation, the duct mode number is truncated as 40 and the beam vibration mode is 25. The comparison

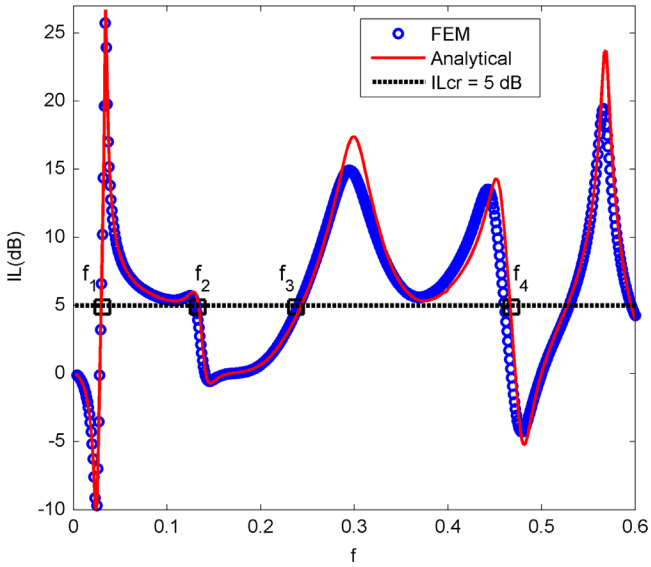

Fig. 2. Comparison between the numerical and the analytical IL in the configuration of $L_c=3$, $m=0.2$, $B=0.0014$, $\sigma=2.7\%$ and $d^*=0.1$ mm.

between the analytical solution for $M=0$ (without flow) and the result from finite element simulation is shown in Fig. 2. The panel has the normalized mass $m=0.2$, the bending stiffness of $B=0.0014$, perforation ratio of 2.7 percent and hole size $d^*=0.1$ mm. The analytical solution is shown as a solid line, and the numerical prediction is given as open circles. There is no visible difference between the two IL spectrum curves at the frequencies $f<0.25$. Although there are some deviations at the peaks and minor frequency shifts at about the spectral peaks, the main concern in the current study is to widen the stopband of the proposed design and to understand the physics behind it by analytical approach and finite element simulation for visualization.

3.1. Parametric study of panel properties

The performance of such device is characterized by the widest stopband that can be achieved. In order to achieve an effective abatement of noise at the first and second blade passage frequency (BPF) at the same time, one stopband or two stopbands covering these two frequencies is the design target. Here two stopbands are defined as the frequency range, $f \in [f_1, f_2]$ in the low frequency range and $f \in [f_3, f_4]$ in the medium frequency range in which the IL is above a criterion level IL_{cr} (see Fig. 2). The IL_{cr} is set as 5 dB which is the maximum IL can be achieved by an expansion chamber with an expansion ratio of 2. Moreover, the cost function for the optimization of the performance is set as the ratio of the band limits $r=f_2/f_1$ and f_4/f_3 to seek for the widest stopband as the BPF of the fan varies. The performance of such MPP housing device depends on many parameters such as geometric configurations of the cavity, length of the panel, structural properties and perforations parameters. In order to begin the investigation of parametric effect, the majority of the variables are fixed first. Aiming to develop a MPP housing device with a compactable geometry to control the ducted fan noise, the cavity is fixed at length $L_c=3$ and height $h_c=0.5$. Results of the performance optimization of the structural properties of the panel without perforations are shown in Fig. 3. Fig. 3(a)–(d) shows the optimal bending stiffness, the maximum bandwidth, and lower and higher band limit as functions of m for the clamped panel. As shown in Fig. 3(b), when the panel mass increases, the

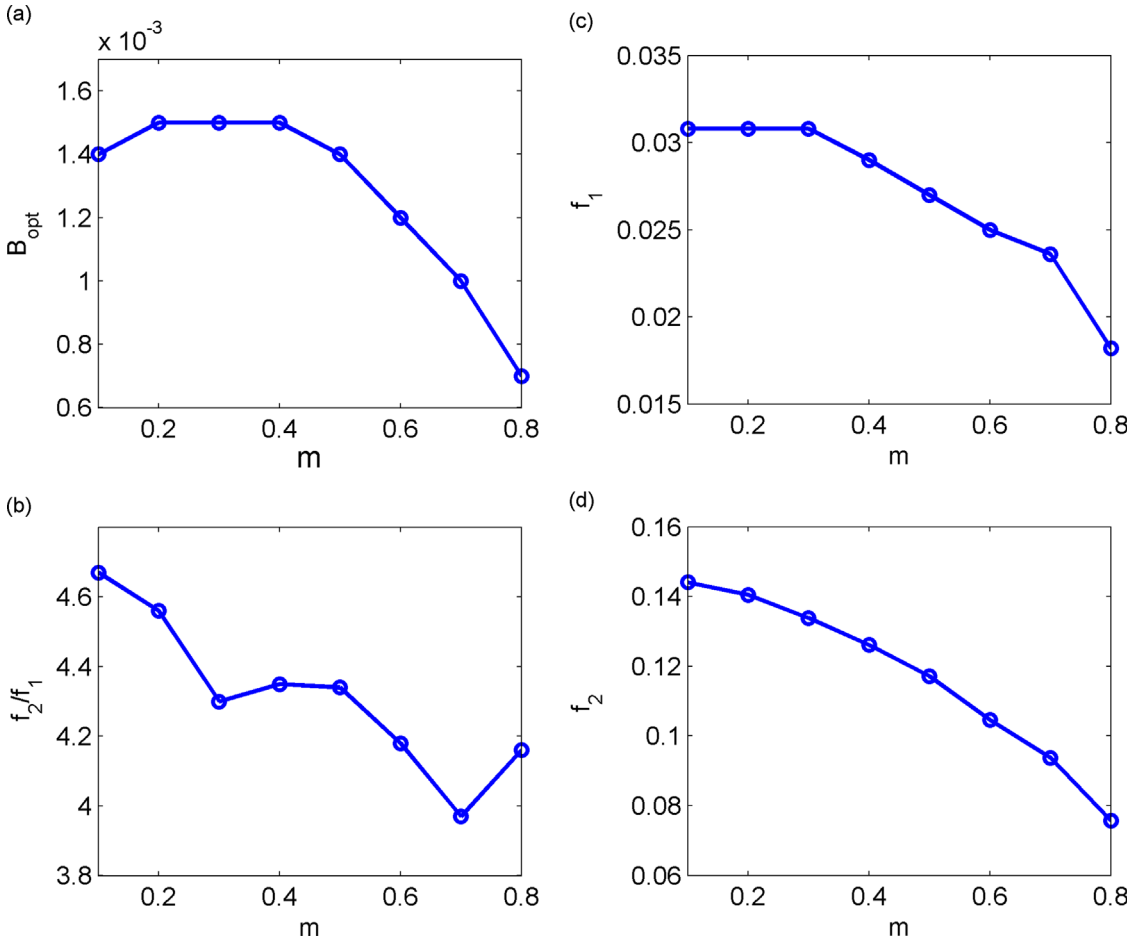

Fig. 3. Performance optimization of the proposed plate housing device without perforations: (a) the variation of the optimal bending stiffness B_{opt} with mass m; (b) the ratio of frequency limit f_2/f_1 in the low frequency range; (c) the dimensionless lower band limit f_1, and (d) the dimensionless upper band limit f_2 varies with mass m.

maximum achievable bandwidth decreases roughly. In the range of $m < 0.8$, the maximum bandwidth can be achieved of at least 3.95. The performance of the proposed device deteriorates as m increases. This is because IL drops below the criterion level for a heavy panel which results in a narrow stopband. Fig. 3(a) suggests that the optimal bending stiffness remains at around $B_{opt}=0.0014$ when $m \le 0.4$ and then gradually falls to a low bending stiffness of $B_{opt}=0.0007$. Roughly speaking, the optimal performance can be obtained under two conditions: $0.0013 \le B_{opt} \le 0.0015$ and $m \le 0.4$. As shown in Fig. 3(d), when the panel mass increases, the upper band limit f_2 decreases too. On the other hand, the lower band limit remains almost the same value $f_1=0.0308$ when $m < 0.3$ and then it decreases as m increases for $m > 0.3$. With seven fan blades and a rotational speed of 4000 rev/min, the dimensionless first and second blade passage frequencies are about 0.14 and 0.28 respectively with respect to the duct height of 0.1 m. In order to control the dominant noise coming from the first and second blade passage frequencies effectively, the upper band limit cannot be lower than 0.14 and hence the optimal mass ratio $m=0.2$ and bending stiffness $B_{opt}=0.0014$ are chosen.

With the mass ratio fixed at $m=0.2$ and bending stiffness of $B=0.0014$, other influential parameters such as perforated ratio and hole size of the MPP have to be varied in order to optimize the performance. Fig. 4(a) shows the comparisons of IL of the proposed device with various hole sizes of the MPP when the perforation ratio is kept at 1 percent. When the dimensional diameter of the hole $d^*=0.1$ mm, two peaks at the frequency range of $f=0.04$–0.14 are observed. When the dimensional diameter is increased to 0.3 mm or 0.5 mm, the trough point between f_1 and f_2 gradually falls below the criterion level IL_{cr}. It results in a very narrow stopband for 5 dB as the criterion level. When the diameter of the orifice of MPP is increased, the acoustic resistant $Z_{i,resist}$ is decreased while the acoustic reactance $Z_{i,react}$ of MPP is slightly increased. This leads to the increase of the coupled structural impedance and thus the response of the MPP at the second and fourth mode is reduced accordingly and the capability for sound cancellation at the frequency about $f=0.14$ is reduced. Fig. 4

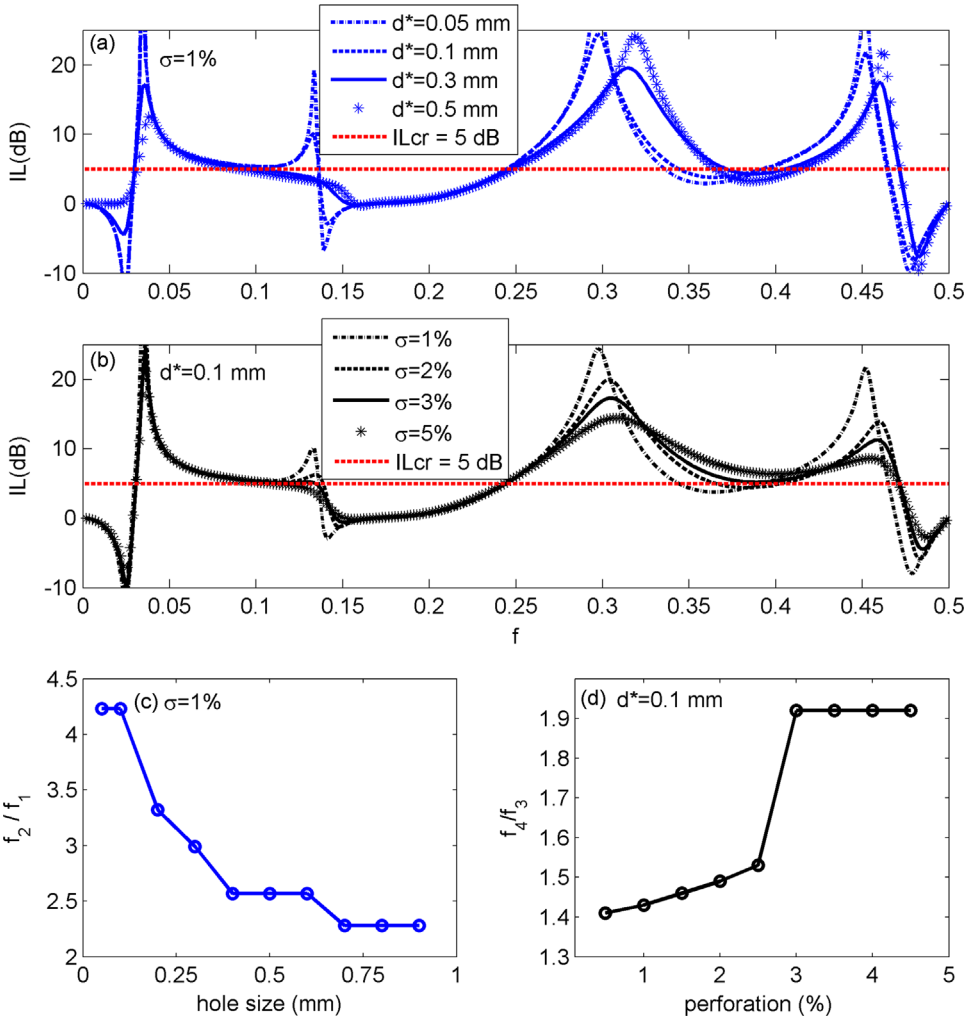

Fig. 4. Performance optimization of the proposed MPP housing device: (a) the IL spectrum with different hole size and the fixed perforation ratio of 1%; (b) the IL spectrum with different perforation ratio and the fixed hole size of $d^*=0.1$ mm; (c) the ratio of frequency limit f_2/f_1 in the low frequency range as a function of hole size of MPP and (d) the ratio of frequency limit f_4/f_3 in the high frequency range as a function of perforation ratio.

(b) shows the variation on the IL spectrum for different perforation ratios when the diameter of holes is fixed at 0.1 mm. When the perforation ratio varies from 1 percent to 3 percent, the second peaks slightly drops but it has no noticeable influence on the stopband in the frequency range of $f=0.04$–0.14. On the other hand, the trough point at frequency around $f=0.4$ rises with the increase of perforation ratio such that the stopband is widened in the frequency range of $f=0.24$–0.48. This means that the effect of perforation may be beneficial for widening the stopband in the medium frequency range. Besides, the third and fourth peak of IL is shifted to higher frequencies. This behavior is similar to the shift of the curve of normal incidence sound absorption coefficient when the perforation ratio is increased due to the reduction of the reactance [11–13]. The increase of perforation ratio reduces both the acoustic resistance and inertia reactance of MPP thus the resonance frequency will be shifted to high end of frequency spectrum. Fig. 4(c) shows the stopband ratio of f_2/f_1 as a function of hole size of perforation while Fig. 4(d) depicts the stopband ratio of f_4/f_3 as a function of perforation ratio. Roughly speaking, the stopband ratio f_2/f_1 decrease monotonically with the diameter of the holes when the diameter increases from 0.1 mm as shown in Fig. 4(c). Fig. 4(d) shows that the stopband ratio f_4/f_3 grows from about 1.4 to 1.92 and then remains constant when the perforation ratio reaches 3 percent. Therefore the optimal perforation and diameter of the hole of MPP housing device is about 3 percent and 0.1 mm respectively.

3.2. Performance and sound suppression factor

Fig. 5(a) compares the IL performance of the proposed device with and without a plate and a plate with micro-perforations as well as the membrane housing introduced by Liu et al. [23] in case of no flow ($M=0$). The IL curve of the proposed plate housing without perforations with $B=0.0014$, previously determined as the optimal bending stiffness is shown as the dashed line. Two peaks are observed at the low frequencies, which are caused by the sound cancellation between the radiated sound from the dipole source with an anti-phase relationship and radiated sound from the panels. The stopband begins from $f_1=0.03$ and ends at $f_2=0.14$, corresponding to $f_2/f_1=4.7$. Besides, the third peak is observed in the middle frequency range and the stopband ranges from $f_3=0.246$ to $f_4=0.33$, corresponding to $f_4/f_3=1.34$. With these two stopbands in the low and middle frequency range, the proposed device with a panel is effective for controlling the ducted fan noise with the first and second blade passage frequency range of $f=0.12$–0.14 and $f=0.24$–0.28 respectively. When perforation ratio of $\sigma=3$ percent and dimensional diameter $d^*=0.1$ mm are introduced into the panel, the second peak slightly drops but the width of stopband undergoes no noticeable change. The trough point between the third and fourth peak lift up so that a wide stopband $f\in[0.24, 0.485]$ of 5 dB is obtained. It is beneficial for controlling the fan noise at a wider working band of first and second blade passage frequencies. Compared with the tensioned membrane housing the dipole source with the same cavity height, the MPP housing device achieves a lower frequency limit at $f_1=0.03$ such that the

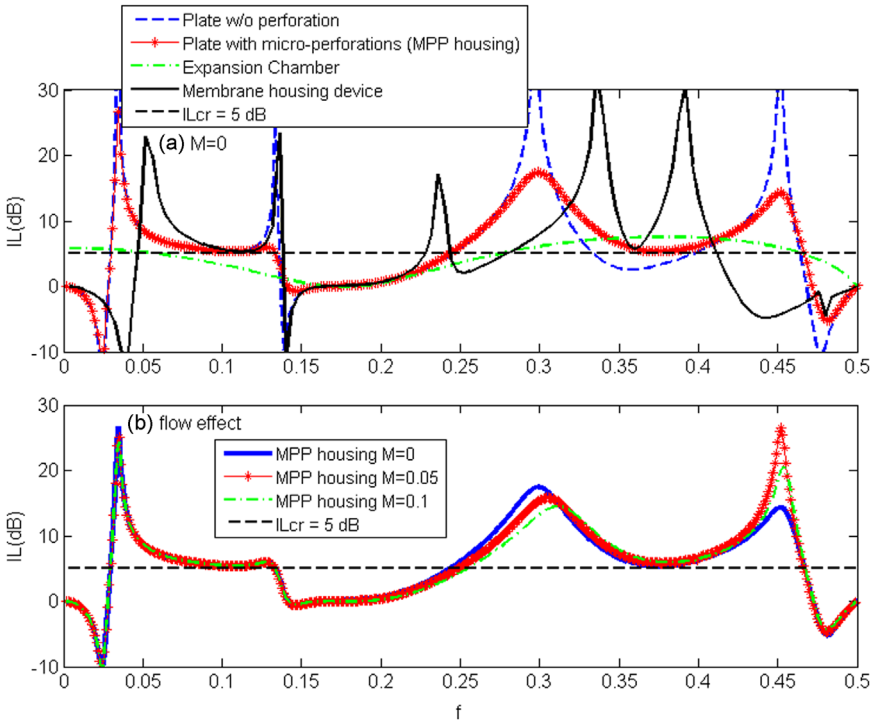

Fig. 5. Performance of different kinds of silencing device: (a) Comparison of the IL spectra among the plate housing device, MPP housing device with optimal parameters, the expansion chamber and membrane housing device in same configuration for controlling dipole source without flow and (b) the performance of MPP housing with and without flow.

stopband at the low frequency region has an encouraging improvement. In addition, the stopband in the middle frequency range is also widened. When there is flow, the impedance of MPP varies and hence the response of the MPP changes accordingly. This leads to the change of vibroacoustic coupling among the MPP, acoustics fields in both the cavity and duct. Fig. 5(b) compares the performance of MPP housing with and without flow. The curves of insertion loss for $M=0$, $M=0.05$ and $M=0.1$ have no noticeable change at the low frequency range $f<0.17$. The low limit frequency f_3 of the second stopband is shifted towards the high end of frequency spectrum slightly when the flow effect is considered. The acoustic resistance in Eq. (4) is increased with the flow rate and it will enhance damping on the system such that the maximum of IL is reduced accordingly [15]. Apart from this, the positive reactance of Eq. (5) is reduced when the flow rate is increased. It behaves as the reduction of the massive effect on the MPP housing so the third and fourth peak of IL is shifted to high frequency regime. This results in a narrower effective frequency range of controlling the second blade passage frequency. Nevertheless, the proposed device can still effectively control the fan noise with the first and second blade passage frequency range of $f=0.125$–0.14 and $f=0.25$–0.28 respectively.

In order to understand the physics behind of the formation of the IL trough and peak in the IL spectrum, the sound radiation efficiency is employed to assess the sound radiation ability of a sound source inside various kinds of housing. In addition, a sound suppression factor is introduced to examine the noise restrain effect of the silencing device. The sound radiation efficiency [32] is investigated through sound suppression factor (F_s) which is defined as

$$F_s = 1 - \frac{W_{sil}}{W_{str}} \tag{21}$$

where W_{str} and W_{sil} are the sound power at the outlets of straight duct and silencing device respectively. Fig. 6(a) shows the IL spectrum comparison among expansion chamber (dotted line), plate housing without perforations (dashed line) and with micro-perforations (solid line with star). Fig. 6(b) and (c) shows total sound power radiation and sound suppression factor respectively. As shown in Fig. 6(b), the sound power radiated from the dipole source in a straight duct remains at about 25 W for all frequencies while that in the expansion chamber, plate housing device and MPP housing device vary at different frequencies. For the plate and MPP housing device, the sound power radiated out is very high in the frequency range of around $f=0.024$ and $f=0.14$ in which negative IL is obtained. This means that the sound radiation from MPP or plate is too strong to deteriorate the performance of MPP housing when the dipole source is excited. On the other hand, at the peak of IL, the sound power radiation from plate housing device is almost zero and it means that almost all the sound undergoes sound cancellation. When the microperforation is added, the response of the plate is affected so that the sound power radiation from MPP housing device is not zero. Besides, there is about 70 percent deduction of sound power radiation for MPP housing device in the frequency range of [0.03, 0.13] and [0.24, 0.48] that leads to the positive IL. This also results in a high value of sound suppression factor as shown in Fig. 6(c). Generally speaking, the sound power radiation of the MPP housing device is lower than that of the plate housing device in the middle frequency range of $f=0.33$–0.4 but the corresponding suppression factor is increased. This probably implies that the sound cancellation capability between the MPP and dipole sources is reduced but it is compensated by the enhancement of sound absorption by the MPP. Therefore IL is increased at this frequency range.

3.3. Modal analysis

In order to further investigate the trough points of the IL spectrum contributed by the MPP housing device, the modal response of the MPP at the optimal performance ($m=0.2$, $B_{opt}=0.0014$) is studied. In Fig. 7, the IL spectrum is demonstrated on the top row. The vertical dashed lines present the position of trough points in the IL spectrum for reference. The four rows below illustrate the responses of the first four modes of velocity amplitudes respectively. The higher order modal responses are rather weak, so only the first four modes are analyzed. The second and fourth modal responses were much higher than the odd mode at $f=0.024$ according to Fig. 7(a)–(d). And the magnitude of the second modal response is the highest among them. This means that the second mode is dominant at this frequency which leads to a very strong sound radiation to the outlet of the duct and thus insertion loss is negative. At trough points of IL at $f=0.14$ and at $f=0.48$, there are peaks in the second mode $|V_2|$ and fourth mode $|V_4|$ respectively. Moreover, the fourth modal response is dominant for the IL trough at $f=0.14$ while the first two even modes contributes to the third trough of IL at $f=0.48$ with an equal weighting of influence. Generally speaking, the plate response is dominated by the even modes of the vibration due to the dipole source nature and the trough points are attributed to the too strong radiation of the sound from the plate to the outlets of the duct.

3.4. Sound intensity visualization

In order to understand the sound field distribution at the frequency of trough and peak points, sound intensity vectors $\left(\vec{I}=\frac{1}{2}\mathrm{Re}\left(p\vec{v}^{*}\right)\right)$ [33] are visualized in Fig. 8. The first row shows the real intensity field in the MPP housing device and the second row is the "normalized" vector fields which can show the directional nature of the intensity field with the same magnitude. Fig. 8(d) shows the phase difference of the intensity flow between the cavity and duct in the black circle region of intensity field and gives a clearer image of the in-phase and anti-phase of intensity flow. At the trough point of IL at $f=0.024$, Fig. 8(2a) indicates that the energy flow in the cavity starts from the center to the MPP leading edge (left-hand side and upstream) and trailing edge (right-hand side and downstream), and then converges with the sound waves from the

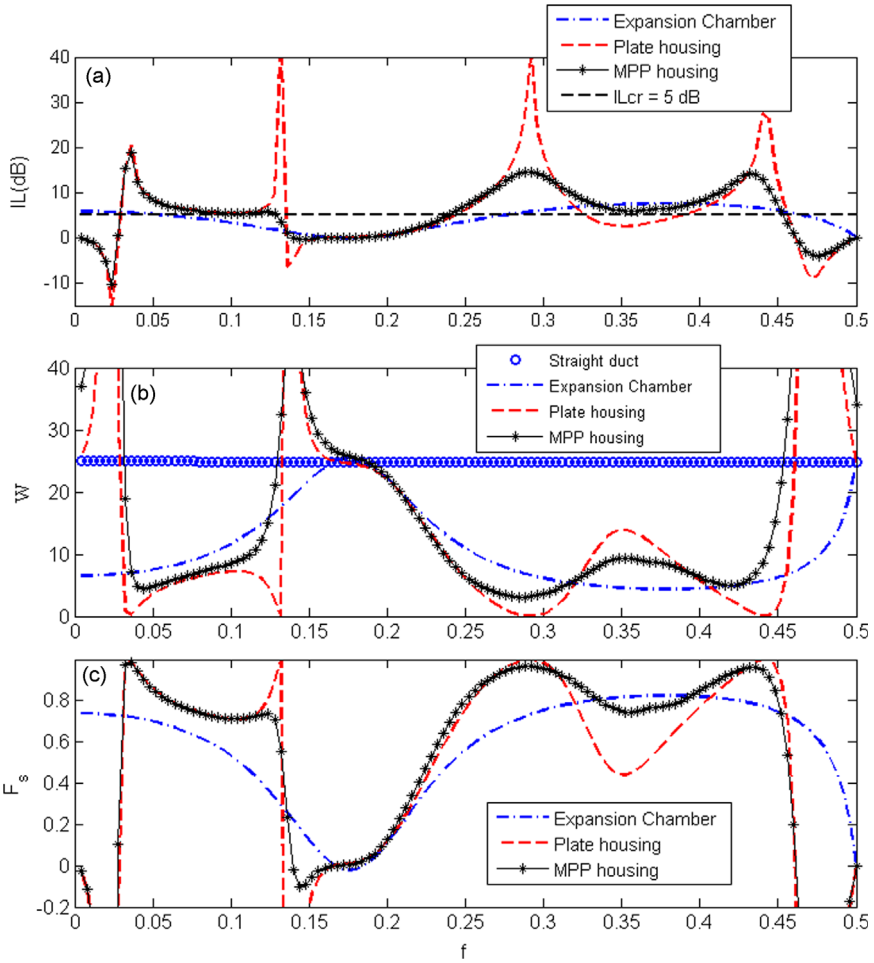

Fig. 6. Sound radiation and sound suppression factor: (a) the comparison of IL spectrum comparison among expansion chamber, plate housing device and MPP housing device; (b) sound radiation power of dipole source in different silencing housing device and (c) sound suppression factor for different silencing housing device.

dipole source and transmits to two outlets of the duct. As the energy flows in the cavity and in the duct at the leading or trailing edge of MPP dominantly point towards the outlet direction, the acoustic energy to the outlet is reinforced and hence there is almost no abatement of noise radiation from the dipole source. For the first peak point (f=0.036) of IL as shown in Fig. 8(2b), the energy flow in the cavity also converges with that from the duct, but the two energy flows are close to anti-phase with the phase difference of 120° as shown in Fig. 8(d). This results in sound cancellation to a certain extent. Therefore there is less energy transmitted to the outlet at f=0.036 as shown in Fig. 8(1b) compared with Fig. 8(1a). Regarding the third peak of IL as shown in Fig. 8(2c), in the middle of the cavity, the intensity vectors seem to be in the opposite directions and result in sound cancellation expected inside the cavity. Generally speaking, at the trough point of IL, the radiation sound intensity to the duct converges with that from the dipole source with almost in-phase relationship and thus the sound at the outlet is reinforced. At the peak point of IL, the phase difference between the radiated sound intensity from the panel and that from the dipole source is greater than 90° at the leading or trailing edge of the panel and this leads to cancellation of the sound to some extent.

3.5. *Monopole and dipole source comparison*

The operation of a real fan may have a dipole and monopole nature, so the performance of the MPP housing device to reduce the monopole and dipole source is investigated. Fig. 9(a) compares of the IL of MPP housing device (σ=2.7 percent and d^* 0.1 mm) to control the monopole and dipole source with the same sources strength. With the same property of the MPP, the IL for controlling the monopole is higher than that for controlling the dipole at the frequency from f=0.12 to f=0.23. On the other hand, the MPP housing device for controlling the dipole outperforms controlling the monopole source at the low frequency range of f=0.03–0.14 and at the relatively high frequency range of f=0.24–0.485. Although the MPP housing device for controlling the monopole source does not perform better than controlling the dipole at low frequencies,

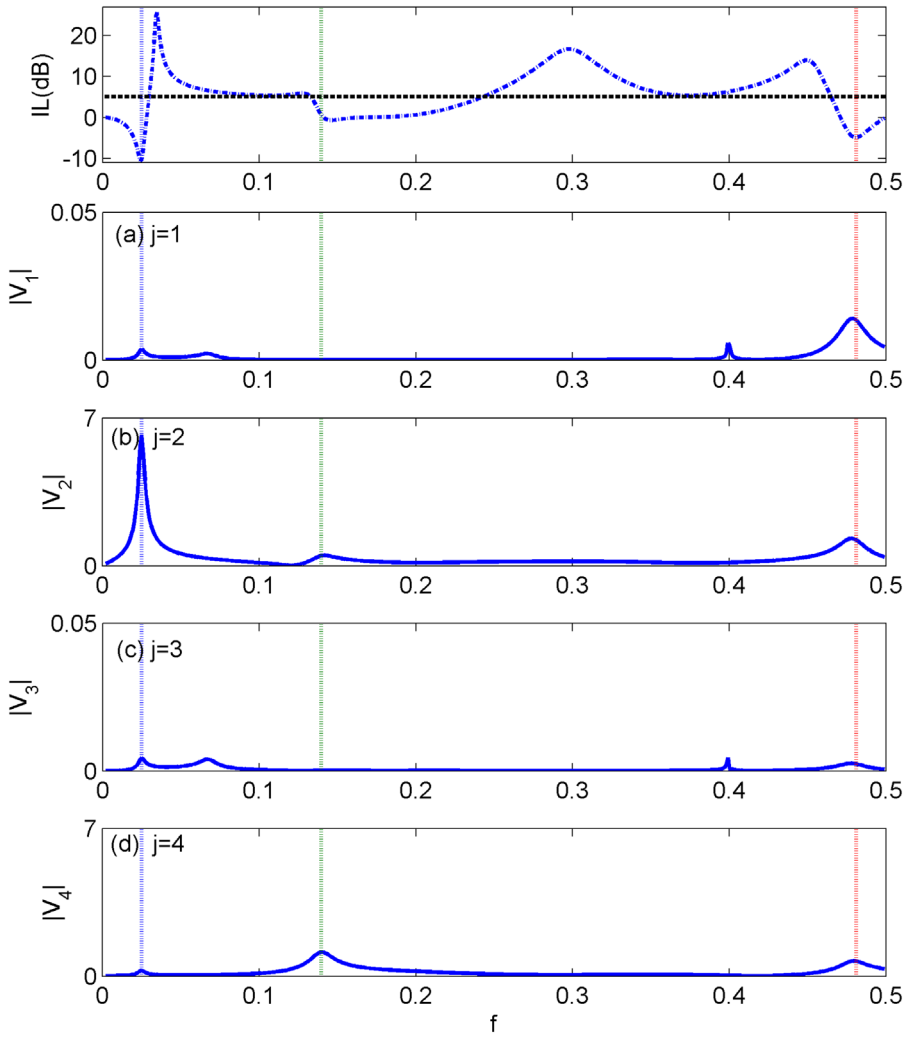

Fig. 7. Modal radiations. The top figure is the IL spectrum of MPP housing device (m=0.2, B=0.0014 with perforation ratio of 2.7% and d^*=0.1 mm): (a)–(d) corresponds to the first four modal amplitude$|V_j|$.

it works effectively at a wide stopband in the middle frequency range. Fig. 9(b), (c) and (d) shows the panel vibration response at different frequencies of f=0.124, f=0.208 and f=0.356 respectively. For the dipole source, the response of the panel at f=0.124 which is the IL peak appears to be higher than that at other frequencies. For the monopole source, odd modes are dominant and the vibration of the panel at frequencies f=0.124 and f=0.208 is stronger than that at f=0.356 which is at the trough of IL. The performance of such silencing device is dramatically influenced by the nature of the sound source. Therefore the source characteristics should be taken into account in the design stage of such silencing device.

4. Experimental validation

Having obtained the result from the finite element method and theoretical analysis, an experiment was conducted to validate the proposed 2D theoretical model. The experimental setup [26] is illustrated in Fig. 10. The experiment was carried out in an anechoic chamber with dimension of 6 m × 6 m × 3 m. The duct used had a dimension of h^*=100 mm by w^*=100 mm cross-section, with a total length of 620 mm. Two pieces of MPP which had a length of $L_c{}^*$=3 h^*=300 mm, were placed at two sides of the center segment of the duct and both covered with a cavity of depth $h_c{}^*$=50 mm. The ratio of the plate to air mass calculated by $(m^*/\rho_0^* h^*)$ was 0.98. In order to achieve the condition of light weight, the material of MPP was composite plate which was made of polymethacrylimide (PMI) with reinforcement of one carbon fiber tow and the microperforated holes were drilled by a laser machine. The number of carbon fiber tows attachment varies the bending stiffness of MPP [34]. The first cut-on frequency in the duct which is made of Acrylic is about 1700 Hz. As shown in Fig. 10, a

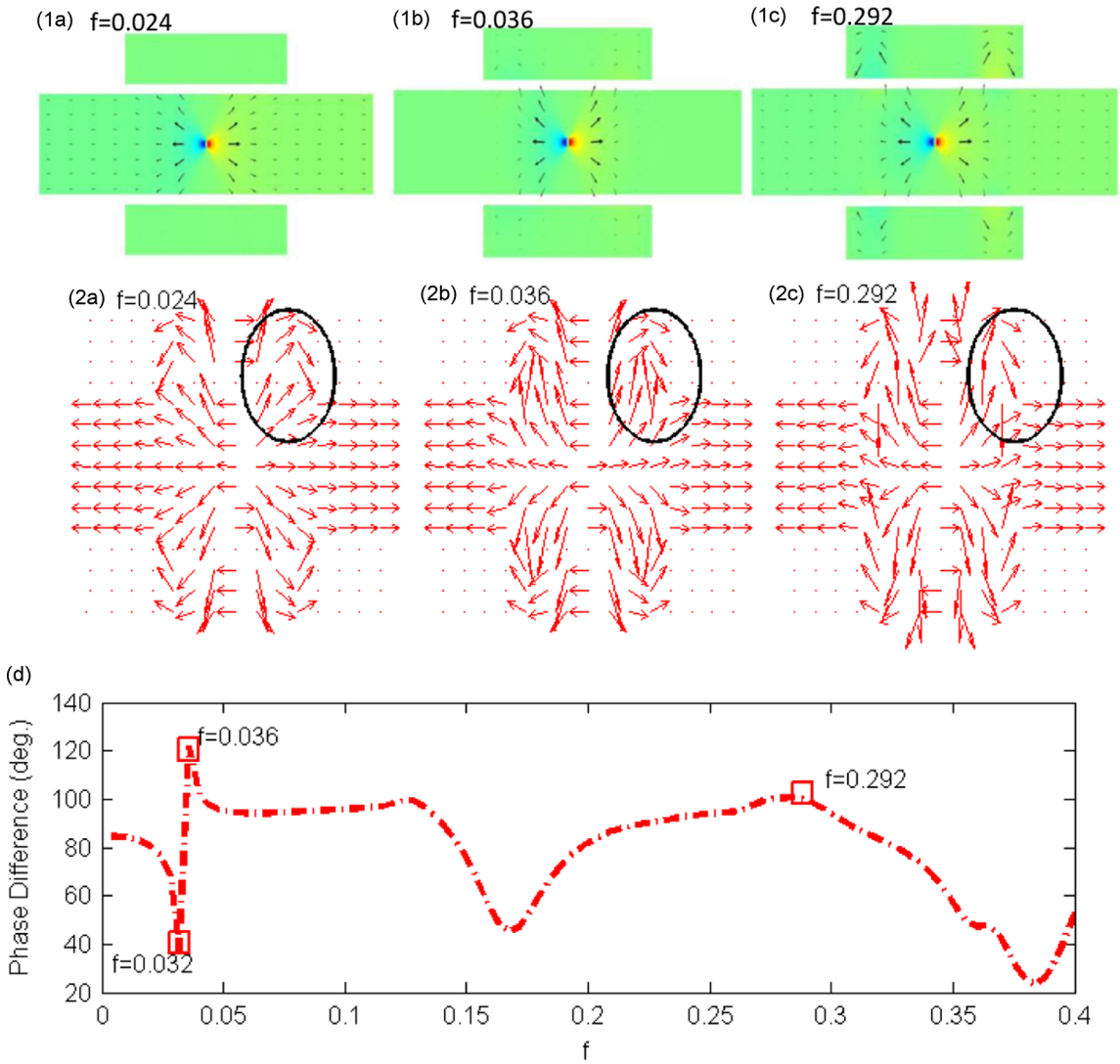

Fig. 8. Sound intensity distribution. The first row is the real intensity field while and the second row corresponds to the "normalized" vector field. (1a) and (2a) show the results at f=0.024; (1b) and (2b) show the results at f=0.036; (1c) and (2c) the results at f=0.292. (d) The angle difference of the sound intensity flow in the cavity and duct at the trailing edge of the MPP.

small loudspeaker of 40 mm in diameter was utilized to simulate the dipole sound source. The loudspeaker was held as a cantilever by a very rigid rod and located at the center of the duct. The radiated noise was measured both at 282.8 mm upstream and downstream outlets of the duct with an angle of θ=45° from the near-side duct opening plane. One pair of 1/2-in. microphones type B&K 4189 are used and supported by Nexus Conditioning Amplifier type B&K 2693. The loudspeaker was driven by a function generator Hioki 7075 via an Audio power amplifier Crest LA 1201 with white noise. The signals from the microphones were acquired through an analog-to-digital converter (NI DAQ card 9234 in the box of NI 9162) with the MATLAB program. Finally, the sound pressures were directly measured at the exits at the upstream and downstream duct, denoted by p_{up} and p_{dn}, respectively. In reality, the radiation from the loudspeaker is not a pure dipole. Reflected sound is also scattered by the loudspeaker surface and junctions between the interface at the rigid wall and MPP. The sound radiation from the noise source is considered to consist of one dipole with anti-phase relation and one monopole with in phase relation. Besides, the measurement at one point at the upstream outlet will be contaminated by the sound pressure at the downstream outlet. Therefore, extraction of the dipole component from the real noise source is necessary during the signal processing. The sound wave decomposition procedure was developed by Huang et al. [3]. The acoustic pressure component at the outlet of the duct can be expressed as a function of the reflection coefficient of the open ends β, and the pressure ratio between p_{up} and p_{dn}. The net sound pressure of the dipole component at the upstream side which is denoted

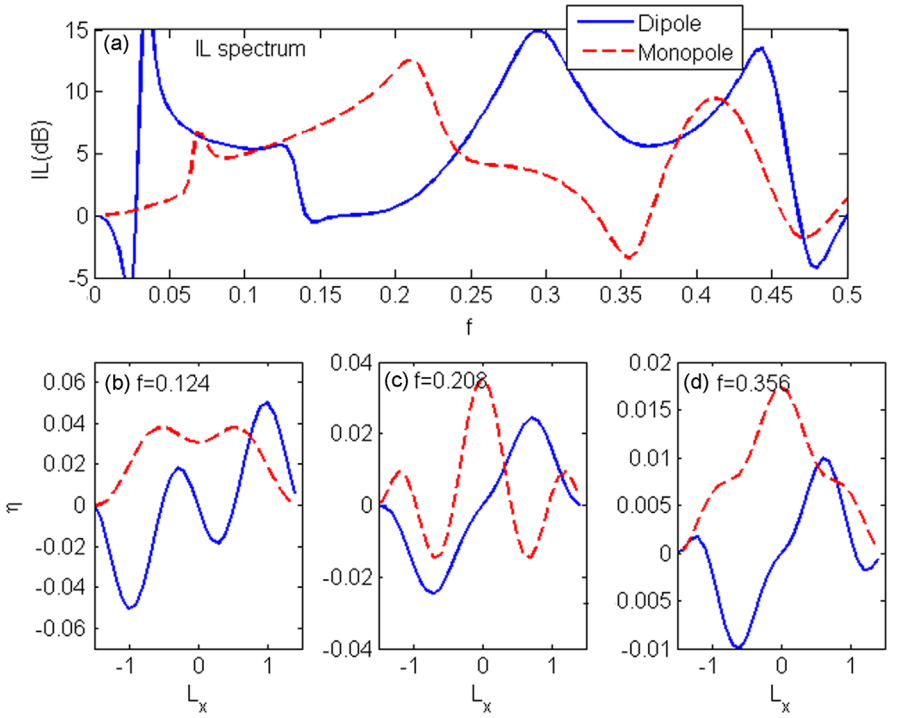

Fig. 9. Performance of MPP housing device for different kinds of sound source: (a) comparison of IL spectra of the proposed device between the dipole source and the monopole source. Vibration response of the MPP at (b) $f=0.124$; (c) $f=0.208$ and (d) $f=0.356$.

as p_{ud} after decomposition is given as

$$p_{ud}=\frac{p_{up}(e^{ikL}+\beta)\left[1-\left((p_{dn}/p_{up})-\gamma\right)/\left(1-\gamma(p_{dn}/p_{up})\right)\right]}{2e^{0.5ikL}(1+\beta)\left[1+\gamma\left((p_{dn}/p_{up})-\gamma\right)/\left(1-\gamma(p_{dn}/p_{up})\right)\right]},$$
$$\beta=\frac{Z_{open}-1}{Z_{open}+1}\ \text{and}\ \gamma=-(r/r_{far})^2\left(\frac{L_t+r\cos(\theta)}{r\cos(\theta)}\right)e^{-ik_0(r_{far}-r)} \tag{22}$$

The corresponding insertion loss (IL) for the net dipole radiation can be obtained:

$$\mathrm{IL}=10\log_{10}\left(\frac{|p_{ud}|^2{}_{str}}{|p_{ud}|^2{}_{MPP}}\right)$$

where Z_{open} is the open-end impedance, r and θ are the distance and angle between the microphone and the near-side duct opening (upstream side) respectively as shown in Fig. 10. r_{far} is the distance between the microphone and the far-side duct opening (downstream side). L_t is the total length of the whole test rig from the opening at upstream side to another opening at the downstream side. As shown in Fig. 10, the position of the microphone in the current experiment is set to be $r=282$ mm, $\theta=45^\circ$ and $r_{far}=774.4$ mm and total length of the whole test rig is $L_t=620$ mm.

A comparison was made between the theoretical prediction and experimental data for the plate housing device and MPP housing device ($m=0.98$, $B=0.0056$, $d^*=0.5$ mm and $\sigma=2.7$ percent) for the loudspeaker as pure dipole source respectively as shown in Fig. 11. Although the structural property and perforation property of the plate and MPP in the experiment were not optimal, the purpose of experiment was to validate the theoretical model. For the measurement, the lower limit frequency was 150 Hz due to the limitation of the radiation capability of a small loudspeaker which acts as a dipole source while the upper limit was 1700 Hz which is the cut-on frequency of the duct. Fig. 11(a) depicts that IL performance of the MPP housing device outperformed the plate housing device experimentally in the middle frequency range of 1000–1500 Hz. By introducing perforations with small holes on the plate, the IL performance was enhanced in the middle frequency, which matches the parametric study in Section 3.1. The measurement has been done for about five times with the accuracy of about ± 0.5 dB. When the microphone position varies with about 1 percent in radius r and θ, the variation of the insertion loss is about 0.15 dB. Besides, we also found that the change of bending stiffness within 1 percent results in the variation of insertion loss of about 0.08 dB. Overall deviation induced by the microphone position and structural property of the plate is not very significant in the current study. The comparison between the theoretical prediction and experimental results is depicted in Fig. 11(1b) and (2b) for the plate and MPP housing device respectively. The experimental data with dipole extraction are depicted by open circles while the numerical prediction of IL for the pure dipole source is presented by solid

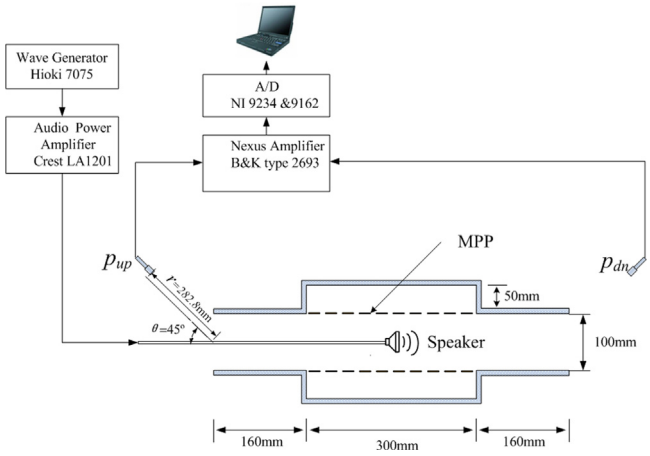

Fig. 10. Experimental setup for measuring the actual sound pressure radiated at the outlet by using two microphones at two exits of the duct.

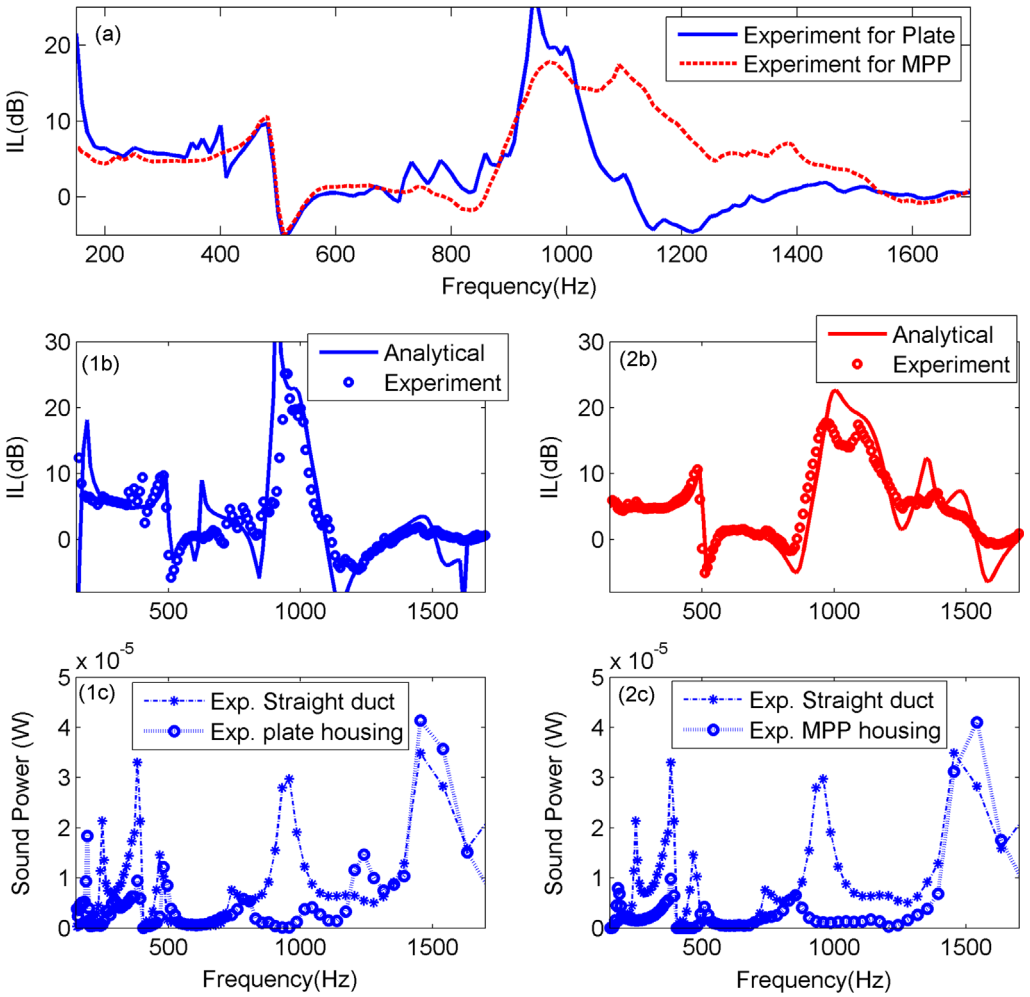

Fig. 11. Experimental validation: (a) the experimental results of IL for plate housing device (B=0.0056, m=0.98) and MPP housing device (B=0.0032, m=0.98, σ=2.7% and d^*=0.5 mm); (b) the comparison between analytical prediction and experiment measurement for (1b) plate housing device and (2b) MPP housing device and (c) the comparison of experimental results of sound power radiation from the loudspeaker between straight duct and silencing device; (1c) is plate housing and (2c) is MPP housing.

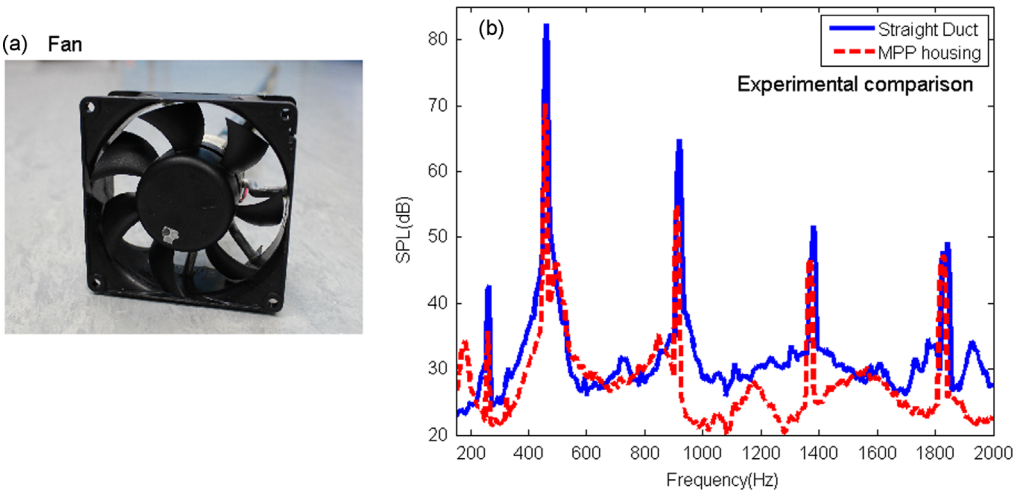

Fig. 12. Experimental investigation of MPP housing controlling a real fan noise: (a) the real fan with 7 fan blades and (b) the comparison of experimental results of sound pressure level of real fan in straight duct and in MPP housing.

lines. Roughly speaking, the experimental data agree with the numerical prediction in terms of the overall IL level and the spectral pattern, although the experimental result is smoothed at the peak and trough points. On average, the IL is about 5 dB in the frequency range of 150–500 Hz and 850–1100 Hz for the plate device. When micro-perforation is added into the plate, the performance in the middle frequency range obviously improved with a wider effective stopband. Hence, the low and middle frequency ranges are expected to cover the first two blade passage frequencies (BPFs) of fan noise in the ventilation system with a rotation speed around 4000 rev/min and a seven-blade fan. In order to examine the sound power radiation of the loudspeaker with both dipole and monopole feature by using the proposed silencing device, sound intensity measurement by sound intensity probe (B&K 2682) at the outlets of the duct was conducted in the anechoic chamber. There were 25 measuring positions associated with equal areas on the surface of the each outlet of the duct. The sound power which can be determined by integrating the product of sound intensity and the corresponding surface area is depicted in Fig. 11(1c) and (2c) for the plate and MPP housing device respectively. Roughly speaking, MPP housing device performs better than plate housing for the suppression of sound power radiation from the loudspeaker with both the dipole and monopole feature in the frequency range of 200–1400 Hz.

5. Performance of MPP housing on an axial fan

In order to examine the performance of the MPP housing when there is mean flow, a real axial fan with seven fan blades, 20 mm chord length and 90 mm diameter is inserted into the testing rig. The setup of the experiment is similar to speaker test illustrated in Fig. 10. The difference is the type of sound source. Here, the fan is driven by a DC power supply (TRIO PR-654). Fig. 12(a) shows the front view of the fan rotor. The rotational speed is monitored by a tachometer to determine the BPFs of the fan. The axial fan is located at the center of MPP housing operating with rotation speed of 3840 rev/min and mean flow of 6.4 m/s. The corresponding first two BPFs are 448 Hz and 896 Hz. Fig. 12(b) shows the SPL measured with the extraction of the dipole component for the straight duct (solid line) and that for MPP housing (dashed line). By the utilization of MPP housing, the dominant noise at first two BPFs are reduced by about 10 dB, which will be beneficial for the noise control of domestic product. At the meantime, the flow speed and pressure drop measurement are carried out. It is found that the flow speed at the outlet of MPP housing is maintained at about 6.4 m/s and the pressure drop (0.5 percent) is small enough to be negligible. Therefore, the MPP housing device can control the first two BPF noise of a fan in the designed frequency range with a compact geometry and with negligible pressure drop.

6. Conclusions

A two-dimensional theoretical model for in-depth understanding of vibro-acoustic coupling between the vibrating MPP and the sound fields of a duct and backed cavities with a dipole sound source excitation has been established. The theoretical results have been validated by both finite element simulation and experiment. The optimization process has been conducted on several parameters such as the panel mass, bending stiffness and perforation properties. The noise reduction mechanism has been investigated through modal analysis, sound source radiation ability and sound intensity field study. The excitation source was changed from a dipole to a monopole in order to examine the feasibility of controlling the sound sources of different nature by the MPP housing device. The major conclusions that can be drawn are as follows:

(1) In the configuration of the MPP housing device with the cavity length of $L_c=3$ and cavity height of $H_c=0.5$, with optimal structural bending stiffness of $B=0.0014$, mass ratio $m=0.1$, perforation ratio of $\sigma=2.7$ percent and diameter of the hole $d^*=0.1$ mm, 70 percent of the sound radiation from the dipole source can be suppressed in the desirable normalized low frequency range of $f=0.03$–0.14 and simultaneously at the normalized medium frequency of $f=0.24$–0.485. When the dipole source is replaced by a monopole source, the MPP housing device can work effectively only in the frequency range of $f=0.06$–0.2.

(2) The panel vibration induced by the dipole source radiates sound waves to the duct and interacts with the radiation sound waves from the dipole source. Such interaction determines the performance of the silencing device. With the dipole source nature, the second and fourth modes vibrations are dominant and they play a very important role in sound cancellations.

(3) The proposed theoretical model in the two-dimensional configuration has been validated by experiment and there was satisfactory agreement between them. The MPP housing device with compact geometry and an expansion ratio of 2 can achieve larger than 5 dB insertion loss in wide frequency ranges from the low to medium frequency range which cover the first and second BPF noise of a fan-ducted system with corresponding rotation speed. Compared with the tensioned membrane housing device, the MPP housing device can be implemented in a more convenience way practically because the tensile machine is not required.

Acknowledgments

The first author thanks the Hong Kong Polytechnic University for the research studentship and the funding from ME-Choy Yatsze-NSFC-2012, 51205337.

References

[1] H.V. Fuchs, Alternative fiberless absorbers – new tools and materials for noise control and acoustic comfort, *Acoustica* 87 (2001) 414–422.
[2] R. Sugimoto, R.J. Astley, P.B.Murray, Low frequency liners for turbofan engines, *Proceedings of the 20th International Congress on Acoustics*, Sydney, AU, 2010.
[3] L. Huang, X. Ma, L.G. Feng, Suppression of broadband noise radiated by a low speed fan in a duct, *Journal of the Acoustic Society of America* 128 (2010) 152–163.
[4] M.L. Munjal, *Acoustics of Ducts and Mufflers*, John Wiley & Sons, New York, 1987.
[5] M.C. Chiu, Y.C. Chang, Numerical studies on venting system with multi-chamber perforated mufflers by GA optimization, *Applied Acoustics* 69 (2008) 1017–1037.
[6] L. Huang, Modal analysis of a drumlike silencer, *Journal of the Acoustic Society of America* 112 (2002) 2014–2025.
[7] L. Huang, Broadband sound reflection by plates covering side-branch cavities in a duct, *Journal of the Acoustic Society of America* 119 (2006) 2628–2638.
[8] C.Q. Wang, J. Han, L. Huang, Optimization of a clamped plate silencer, *Journal of the Acoustic Society of America* 121 (2007) 949–960.
[9] X.N. Wang, Y.S. Choy, L. Cheng, Hybrid noise control in a duct using a light micro-perforated plate, *Journal of the Acoustic Society of America* 132 (6) (2012) 3778–3787.
[10] D.Y. Maa, Theory and design of microperforated panel sound absorbing construction, *Scientia Sinica* 18 (1975) 55–71. (in Chinese).
[11] D.Y. Maa, Micorperforated panel wideband absorbers, *Noise Control Engineering Journal* 29 (1987) 77–84.
[12] D.Y. Maa, Potential of microperforated panel absorber, *Journal of the Acoustic Society of America* 104 (1998) 2861–2866.
[13] J. Kang, H.V. Fuchs, Predicting the absorption of open weave textiles and micro-perforated membranes backed by an air space, *Journal of Sound and Vibration* 220 (1999) 905–920.
[14] F. Asdrubali, G. Pispola, Properties of transparent sound-absorbing panels for use in noise barriers, *Journal of the Acoustic Society of America* 121 (2007) 214–221.
[15] R. Kabral, L. Du, M. Åbom, M. Knutsson, A compact silencer for the control of compressor noise, *SAE International Journal of Engines* 7 (3) (2014) 1572–1578.
[16] N.S. Dickey, A. Selamet, J.M. Novak, Multi-pass perforated tube silencers: a computational approach, *Journal of Sound and Vibration* 211 (3) (1998) 435–448.
[17] X.D. Jing, X.Y. Wang, X.F. Sun, Broadband acoustic liner based on the mechanism of multiple cavity resonance, *AIAA Journal* 45 (10) (2007) 2429–2437.
[18] Z.B. Lu, X.D. Jing, X.F. Sun, X.W. Dai, An investigation on the characteristics of a non-locally reacting acoustic liner, *Journal of Vibration and Control* (2014).
[19] T. Bravo, C. Maury, C. Pinhède, Sound absorption and transmission through flexible micro-perforated panels backed by an air layer and a thin plate, *Journal of the Acoustical Society of America* 131 (2012) 3853–3863.
[20] T. Bravo, C. Maury, C. Pinhède, Vibro-acoustic properties of thin micro-perforated panel absorbers, *Journal of the Acoustical Society of America* 132 (2012) 789–798.
[21] C.Q. Wang, L. Cheng, J. Pan, G.H. Yu, Sound absorption of a micro-perforated panel backed by an irregular-shaped cavity, *Journal of the Acoustic Society of America* 127 (1) (2010) 238–246.
[22] C.Q. Wang, L. Huang, On the acoustic properties of parallel arrangement of multiple micro-perforated panel absorbers with different cavity depths, *Journal of the Acoustical Society of America* 130 (2011) 208–218.
[23] C.Q. Wang, L. Huang, Y.M. Zhang, Oblique incidence sound absorption of parallel arrangement of multiple micro-perforated panel absorbers in a periodic pattern, *Journal of Sound and Vibration* 333 (2014) 6828–6842.
[24] Y.Y. Lee, E.W.M. Lee, C.F. Ng, Sound absorption of a finite flexible micro-perforated panel backed by an air cavity, *Journal of Sound and Vibration* 287 (2005) 227–243.
[25] A. Putra, D.J. Thompson, Sound radiation from perforated plates, *Journal of Sound and Vibration* 329 (2010) 4227–4250.
[26] Y. Liu, Y.S. Choy, L. Huang, L. Cheng, Noise suppression of a dipole source by tensioned membrane with side-branch cavities, *Journal of the Acoustic Society of America* 132 (3) (2012) 1392–1402.
[27] E. Rodarte, N.R. Miller, *Modeling flow-induced noise of circular cylinders subject to cross flow inside a rectangular duct, Flow Induced Noise in Heat Exchangers ACRC-CR42*, University of Illinois, Champaign, 2001.

[28] D. Takahashi, M. Tanaka, Flexural vibration of perforated plated and porous elastic materials under acoustic loading, *Journal of the Acoustic Society of America* 112 (4) (2002) 1456–1464.
[29] S. Allam, M. Åbom, A new type of muffler based on microperforated tubes, *Journal of Vibration and Acoustics* 133 (2011) 031005-1–031005-8.
[30] P.E. Doak, Excitation, transmission and radiation of sound from source distributions in hard-walled ducts of finite length (I): the effects of duct cross-section geometry and source distribution space-time pattern, *Journal of Sound and Vibration* 31 (1973) 1–72.
[31] L. Cheng, Y.Y. Li, J.X. Gao, Energy transmission in a mechanically-linked double-wall structure coupled to an acoustic enclosure, *Journal of the Acoustic Society of America* 117 (5) (2005) 2742–2751.
[32] G. Squicciarini, D.J. Thompson, R. Corradi, The effect of different combinations of boundary conditions on the average radiation efficiency of rectangular plates, *Journal of Sound and Vibration* 333 (2014) 3931–3948.
[33] D.A. Russell, J. Junell, D.O. Ludwigsen, Vector acoustic intensity around a tuning fork, *American Journal of Physics* 81 (2) (2013) 99–103.
[34] Y.S. Choy, Y. Liu, H.Y. Cheung, K.T. Lau, Development of a composite plate for compact silencer design, *Journal of Sound and Vibration* 331 (2012) 2348–2364.